COVER SHEET

Authors: Shizhong Chen[12]*, Xingxing Duan[12]

Affiliations:

[1] Urumqi Natural Resources Survey, China Geological Survey, Urumqi, Xinjiang 830057, China

[2] Innovation Base of Metallogenic Prediction and Prospecting in Central Asia Orogenic Belt, Urumqi, Xinjiang 830057, China

Correspondence: nanjingcsz@qq.com

Preprint version: v2.0 (July 2026)

Code and data are available at GitHub (https://github.com/peterclogite/R_Critical_Relamination)

and archived at Zenodo under Concept DOI https://doi.org/10.5281/zenodo.20446103 (always resolves to the latest version). This preprint corresponds to Zenodo v2.0

(Version DOI: https://doi.org/10.5281/zenodo.21545544)

R-critical constraints on relamination efficiency: The role of mechanical coupling in continental crust recycling

Shizhong Chen[1,2*], Xingxing Duan[1,2*]

[1] Urumqi Natural Resources Survey, China Geological Survey, 555 Xihuanbei Road, Xinshi District, Urumqi, Xinjiang 830057, China

[2] Innovation Base of Metallogenic Prediction and Prospecting in Central Asia Orogenic Belt, Urumqi, Xinjiang 830057, China

* Correspondence to: Shizhong Chen (nanjingcsz@qq.com; ORCID: 0000-0001-7527-1452) and Xingxing Duan (duanxx@foxmail.com; ORCID: 0009-0006-1017-8373)

Abstract. Continental relamination — the detachment and underplating of subducted continental crust — remains poorly quantified in terms of the mechanical coupling efficiency between the subducting slab and the overriding lithosphere. Here we define R-critical, a dimensionless parameter derived from the competition between buoyancy-driven ascent and viscous resistance at the crust–mantle interface, that quantifies the mechanical coupling required for efficient hybridization. Applied to natural parameter ranges constrained by experimental and observational data, R-critical reveals that efficient mechanical mixing is common but not universal: a substantial minority (~21 %) of the sampled parameter space falls below the critical threshold. Monte Carlo re-estimation (10,000 realizations) incorporating R-critical constraints reduces the effective continent-relamination flux by ~20 % relative to the unconstrained buoyant flux of ~0.35 $km^3\ yr^{-1}$ — the felsic fraction of the ~0.5 $km^3\ yr^{-1}$ continent-collision subduction rate estimated by Hacker et al. (2011, their Fig. 9) — to ~0.28 $km^3\ yr^{-1}$ (cumulative 2.7 Ga volume 7.6×10^8 km^3 vs. 9.5×10^8 km^3 unconstrained). Variance decomposition shows that interface viscosity and strain rate contribute statistically equal and dominant shares (~45 % each), followed by fragment size (~10 %) and density contrast (<1 %) — an exact symmetry imposed by the formulation itself — demonstrating that rheological and tectonic controls on relamination efficiency are of equal first-order importance. The framework generates testable predictions for seismic anisotropy, UHP terrane deformation patterns, and post-collisional magma chemistry, and provides a quantitative bridge between numerical model outputs and experimental petrology inputs.

Short summary. When continents collide, slices of crust can sink into the mantle and later rise back — a process called relamination that helps build and differentiate continents. Whether these crustal slices mix with the mantle or rise back intact depends on a tug-of-war between their buoyancy and the strength of the crust–mantle boundary. We define a dimensionless number, R-critical, that captures this competition and show that mixing is mechanically "gated": in about one-fifth of plausible natural conditions the boundary is too strong and mixing is inhibited. This

lowers the estimated global relamination flux by ~20 % and yields testable predictions for seismic anisotropy, mountain-belt structure, and the chemistry of post-collisional magmas.

1. Introduction

1.1 Background

The recycling of continental crust into the mantle and its subsequent return to the crust — processes collectively termed relamination — has gained increasing attention as a fundamental mechanism of continental evolution (Hacker et al., 2011; Gerya et al., 2004; Kelemen and Behn, 2016). During continental collision, deeply subducted crustal fragments may detach from the downgoing slab and ascend into the mantle wedge, where they interact with peridotite to produce hybrid magmas. These hybrid melts, enriched in crustal signatures, are thought to contribute significantly to post-collisional magmatism and continental growth (Vogt et al., 2013; Gómez-Frutos et al., 2026).

Recent advances in thermomechanical modeling have demonstrated that relamination can reproduce first-order natural observations, including the temporal lag between collision and post-collisional magmatism, and the characteristic geochemical signatures of collision-related igneous rocks (Gómez-Frutos et al., 2026). High-pressure experiments have further validated that crustal compositions, when mixed with peridotite at appropriate pressure–temperature conditions, can indeed generate hybrid melts with geochemically meaningful signatures (Hacker et al., 2011; Kelemen and Behn, 2016).

1.2 The missing link: mechanical coupling

Despite these advances, a critical gap persists between numerical models and experimental petrology. Numerical models output pressure–temperature–time (P–T–t) trajectories and deformation geometries, while experiments require pre-homogenized mixtures as input. The physical process bridging these two scales — mechanical mixing at the discrete crust–mantle interface — has not been quantitatively parameterized.

Natural relamination involves discrete crustal fragments interacting with a peridotite matrix, not the homogeneous mixtures used in experiments. The transition from discrete fragments to hybrid mixtures is governed by mechanical coupling at the crust–mantle interface. Without sufficient mechanical coupling, the experimental starting conditions may never be achieved in nature, regardless of how favorable the P–T conditions appear. This "interface gap" represents a fundamental scaling problem in integrated geodynamic–petrological approaches.

1.3 The R-critical framework

In this study, we introduce the R-critical dimensionless parameter to quantify the mechanical coupling required for efficient hybridization. Drawing analogy from classical dimensionless numbers in fluid and solid mechanics (e.g., Reynolds number, Rayleigh number, Bingham number), R-critical provides a first-order physical threshold for determining when mechanical mixing can bridge the gap between numerical model outputs and experimental inputs.

Our central hypothesis is that relamination efficiency is fundamentally constrained by mechanical coupling, and that a substantial fraction of natural scenarios may fall below the critical threshold required for efficient hybridization. This implies that global relamination fluxes — and consequently the contribution of relamination to continental growth — may be lower than unconstrained estimates suggest (Hacker et al., 2011), because mechanical coupling acts as a gate on efficiency. The R-critical framework transforms the qualitative narrative of relamination into a parameterized, testable model, enabling quantitative assessment of its role in continental crust recycling.

2. Methods

2.1 Definition of the R parameter

The R-critical parameter is defined as the ratio between the characteristic buoyancy force driving mechanical mixing and the viscous resistance opposing it at the crust–mantle interface:

$$R = \frac{F_b}{F_v} = \frac{\Delta\rho \cdot g \cdot L^3}{\eta_i \cdot \dot{\varepsilon} \cdot L^2} = \frac{\Delta\rho \cdot g \cdot L}{\eta_i \cdot \dot{\varepsilon}}$$

where:

- $\Delta\rho$ = density contrast between crustal fragment and mantle (kg m^{-3})
- g = gravitational acceleration (9.81 m s^{-2})
- L = characteristic fragment size (m)
- η_i = effective viscosity of the crust–mantle interface (Pa s)
- $\dot{\varepsilon}$ = characteristic strain rate (s^{-1})

This formulation captures the competition between buoyancy-driven ascent (scaling as L^3) and viscous resistance to deformation and mixing (scaling as L^2), yielding a length-linear dependence for the dimensionless parameter. The physical interpretation is analogous to the Stokes number or Bingham number: it represents the ratio of a driving force to a resisting force, with the critical threshold marking the transition from viscous-dominated to buoyancy-dominated behavior.

2.2 Critical threshold

The critical threshold R-critical is determined by the minimum mechanical coupling required to achieve the hybrid mixing ratios (X_b) observed in natural composite diapirs and experimental products. Based on the analysis of Vogt et al. (2013), who documented composite diapir mixing ratios in the range X_b = 0.4–0.8, we adopt a reference value of:

$$R_{critical} = 10.0$$

This value represents the threshold above which mechanical coupling is sufficient to produce the mixing ratios required for geochemically detectable hybridization. The calibration derives from natural composite diapir systems where mechanical mixing has been independently confirmed through field relationships and geochemical mass balance. We acknowledge that this reference value may vary with specific lithological compositions and P–T conditions (see Sect. 4.5).

2.3 Efficiency model

Relamination efficiency (E) is modeled as a sigmoidal function of the normalized parameter $R/R_{critical}$:

$$E = \frac{1}{1 + \exp\left(-\frac{R/R_{critical} - 1}{w}\right)}$$

where w = 0.3 controls the width of the transition zone. This formulation provides a smooth transition between inefficient ($E \approx 0$) and efficient ($E \approx 1$) relamination regimes, avoiding the unphysical discontinuity of a step function. Alternative formulations (linear and step-function) are provided in the Supplement for comparison and sensitivity analysis.

2.4 Parameter ranges and sources

All physical parameters are constrained by published experimental and observational data (Table 1).

Table 1. Parameter ranges and best estimates used in this study.

Parameter	Symbol	Range	Best estimate	Source
Density contrast	$\Delta\rho$	200–500 kg m^{-3}	300 kg m^{-3}	Crust/mantle density difference (Christensen and Mooney, 1995)
Interface viscosity	η_i	10^{17}–10^{21} Pa s	10^{18} Pa s	Rock deformation experiments (Hirth and Kohlstedt, 2003)
Strain rate	$\dot{\varepsilon}$	10^{-16}–10^{-12} s^{-1}	10^{-14} s^{-1}	GPS measurements (Kreemer et al., 2014)
Fragment size	L	10^3–10^5 m	5×10^3 m	Seismic tomography / field mapping

2.5 Numerical implementation

All calculations were implemented in Python 3.9+ using the NumPy, SciPy, and pandas libraries. The code is structured as follows:

1. Core module (`r_critical.py`): computes R and E for given parameter sets.
2. Efficiency module (`efficiency_model.py`): generates efficiency curves across parameter sweeps.
3. Phase diagram module (`phase_diagram.py`): produces 2-D phase diagrams in parameter space.
4. Monte Carlo module (`monte_carlo.py`): performs the sensitivity analysis, the global flux re-estimation, and the variance decomposition (Spearman-squared primary method and Sobol first-order robustness check).
5. Figure scripts (`figure1.py–figure6.py`): reproduce all figures of this paper.

A unit test suite (59 tests) verifies asymptotic behavior, monotonicity, regime classification, and seed-level reproducibility of all reported results. All code is available at GitHub and Zenodo (see Code availability).

2.6 Timescale estimates for the process hierarchy

The characteristic timescales presented in Fig. 6e are order-of-magnitude estimates derived from standard physical parameters, not empirical measurements. The derivations are as follows:

1. **Mechanical mixing (R-critical):** $t_{mix} \sim 1/\dot{\varepsilon}$, where $\dot{\varepsilon} \sim 10^{-14}$ s^{-1} yields t_{mix} ~ 3 × 10^6 yr. For higher strain rates ($\dot{\varepsilon} \sim 10^{-12}$ s^{-1} in post-orogenic extension), $t_{mix} \sim 10^4$–10^5 yr. The value 10^5 yr represents the order-of-magnitude bound for efficient mechanical mixing.
2. **Thermal equilibration (conduction):** $t_{cond} \sim L^2/\kappa$, where $L \sim$ 10–30 km (crustal fragment scale) and $\kappa \sim 10^{-6}$ m^2 s^{-1} (thermal diffusivity of mantle rocks). This yields $t_{cond} \sim 10^7$–10^8 yr. The value 10^7 yr represents the lower bound for fragments at the kilometer scale.
3. **Chemical diffusion (major elements, solid-state):** $t_{diff} \sim L^2/D$, where $D \sim$ 10^{-18}–10^{-20} m^2 s^{-1} (diffusion coefficients for major elements in silicates at mantle conditions; Zhang, 2010) and $L \sim$ 0.1–1 m (grain to hand-specimen scale for major-element homogenization via solid-state diffusion). This yields $t_{diff} \sim 10^9$–10^{11} yr. Regional-scale (L ~ 100 km) isotopic homogenization requires fluid- or melt-mediated transport with effective diffusivities $D \sim$ 10^{-10}–10^{-12} m^2 s^{-1}, not solid-state lattice diffusion alone.
4. **Seismic detection resolution:** $t_{seis} \sim 10^2$ yr, based on the operational history of global seismic networks (e.g., IRIS, 1984–present) and the minimum time required to resolve an anisotropic signal from noise.

These timescales are intended to illustrate the relative hierarchy of processes controlling relamination, not to provide precise chronological constraints. All values are order-of-magnitude estimates and should be interpreted as such.

3. Results

3.1 R-critical definition and physical interpretation

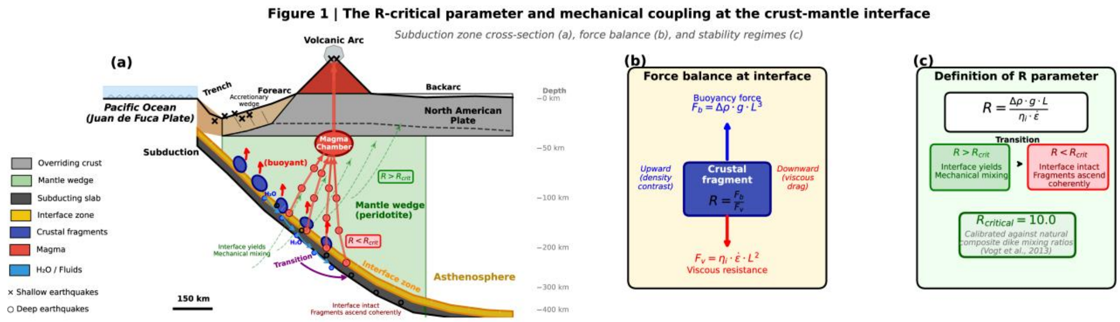

Figure 1

Figure 1. The R-critical parameter and mechanical coupling at the crust–mantle interface. (a)Subduction zone cross-section showing the Cascadia-type convergent margin geometry, with buoyant crustal fragments (blue ellipses) detaching from the subducting Juan de Fuca slab and ascending through the mantle wedge. The yellow interface zone marks the crust-mantle boundary where mechanical coupling is governed by the R-critical parameter. Shallow earthquakes (×) occur in the accretionary wedge; deep earthquakes (○) trace the Wadati-Benioff zone within the slab. H_2O release from slab dehydration triggers mantle wedge melting and magma ascent to the volcanic arc. Green dashed arrows indicate corner flow. The $R > R_{crit}$ regime (shallow, near-trench) corresponds to interface yielding and mechanical mixing; the $R < R_{crit}$ regime (deep) preserves interface integrity and permits coherent fragment ascent. (b) Force balance at the interface: buoyancy force $F_b = \Delta\rho \cdot g \cdot L^3$ (upward, blue) competes with viscous resistance $F_v = \eta_i \cdot \dot{\varepsilon} \cdot L^2$ (downward, red), defining the dimensionless ratio $R = F_b/F_v$. (c) Definition of the R parameter and stability regimes. For $R > R_{critical}$ (=10.0, calibrated against natural composite dike mixing ratios; Vogt et al., 2013), the interface yields and mechanical mixing occurs. For $R > R_{critical}$, the interface remains intact and fragments ascend coherently. The transition between regimes is controlled by interface viscosity η_i , strain rate $\dot{\varepsilon}$, and fragment length scale L .

Figure 1 illustrates the physical meaning of R-critical. The crust–mantle interface acts as a rheological boundary where buoyancy forces (driving mixing) compete with viscous forces (resisting mixing). When $R \geq R_{critical}$, the interface is sufficiently weak to allow mechanical coupling and hybridization. When $R < R_{critical}$, the interface remains too strong, and discrete crustal fragments ascend without significant mixing.

The scaling analysis reveals that:

- buoyancy force scales as $F_b \propto L^3$ (volume-dependent);
- viscous resistance scales as $F_v \propto L^2$ (surface-dependent);

- therefore, larger fragments have a natural advantage in overcoming viscous resistance, but this advantage is counteracted by the higher interface viscosity expected around larger, colder blocks.

3.2 Efficiency curves

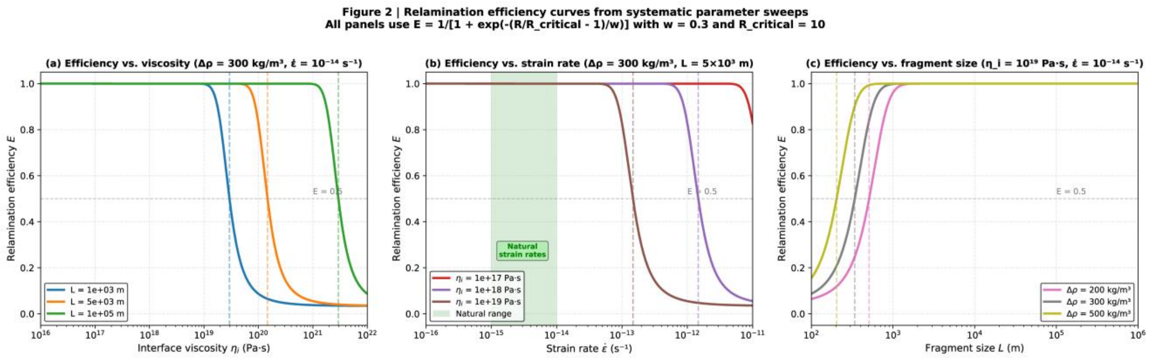

Figure 2

Figure 2. Relamination efficiency curves from systematic parameter sweeps (model predictions). All panels use the sigmoidal efficiency model $E = 1/\left[1 + \exp\left(-\,(R/R_{critical} - 1)/w\right)\right]$ with $w = 0.3$ and $R_{critical} = 10$. Vertical dashed lines mark the parameter value yielding $R = R_{critical}$ for each curve. The horizontal dashed line marks $E = 0.5$ (transition midpoint). (a) Efficiency as a function of interface viscosity for three fragment sizes ($L = 10^3$, 5×10^3, 10^5 m), with $\Delta\rho = 300$ kg m^{-3} and $\dot{\varepsilon} = 10^{-14}$ s^{-1}. Efficiency drops sharply as viscosity increases above 10^{19} Pa s, even for large fragments. The L^3 scaling of the buoyancy force causes larger fragments to maintain higher efficiency at elevated viscosities. (b) Efficiency as a function of strain rate for three interface viscosities ($\eta_i = 10^{17}$, 10^{18}, 10^{19} Pa s), with $\Delta\rho = 300$ kg m^{-3} and $L = 5 \times 10^3$ m. Natural strain rates (10^{-15}–10^{-14} s^{-1}) span the transition zone, indicating strong tectonic control on relamination efficiency. Lower-viscosity interfaces remain efficient across most natural strain rates. (c) Efficiency as a function of fragment size for three density contrasts ($\Delta\rho = 200$, 300, 500 kg m^{-3}), with $\eta_i = 10^{19}$ Pa s and $\dot{\varepsilon} = 10^{-14}$ s^{-1}. Larger density contrasts shift the transition to smaller fragment sizes. Within the natural density range (200–500 kg m^{-3}), efficiency is relatively insensitive to $\Delta\rho$ compared to viscosity or fragment size. (d) R-parameter landscape in interface viscosity–fragment size space ($\Delta\rho = 300$ kg m^{-3}, $\dot{\varepsilon} = 10^{-14}$ s^{-1}). The colour gradient represents $\log_{10}(R)$, with green indicating $R > R_{critical}$ (efficient) and red indicating $R < R_{critical}$ (inhibited). The black dashed line marks $R = R_{critical} = 10$. Natural scenarios: A (continental collision), B (mature subduction), C (post-orogenic extension).

Figure 2 presents efficiency curves generated by systematic parameter sweeps. Key observations:

1. **Viscosity sensitivity:** efficiency drops sharply as interface viscosity increases above 10^{19} Pa s, even for favorable values of other parameters. This reflects the direct inverse proportionality between R and η_i.

2. **Fragment size effect:** larger fragments ($L > 10^4$ m) require significantly lower viscosities to achieve efficient mixing, due to the L^3 scaling of buoyancy forces. However, natural systems may not realize this advantage because larger fragments are typically associated with colder, more viscous interfaces.
3. **Strain-rate dependence:** natural strain rates (10^{-15}–10^{-14} s^{-1}) span the transition zone, implying that local tectonic conditions strongly control relamination efficiency. Post-orogenic extensional regimes with elevated strain rates favor efficient relamination, while stable continental collision zones with low strain rates inhibit it.
4. **Density contrast:** the efficiency is relatively insensitive to $\Delta\rho$ within the natural range (200–500 kg m^{-3}), suggesting that density contrast is not the primary control on relamination efficiency. This is consistent with the observation that crustal compositions vary widely but relamination remains selective.

3.3 Phase diagram

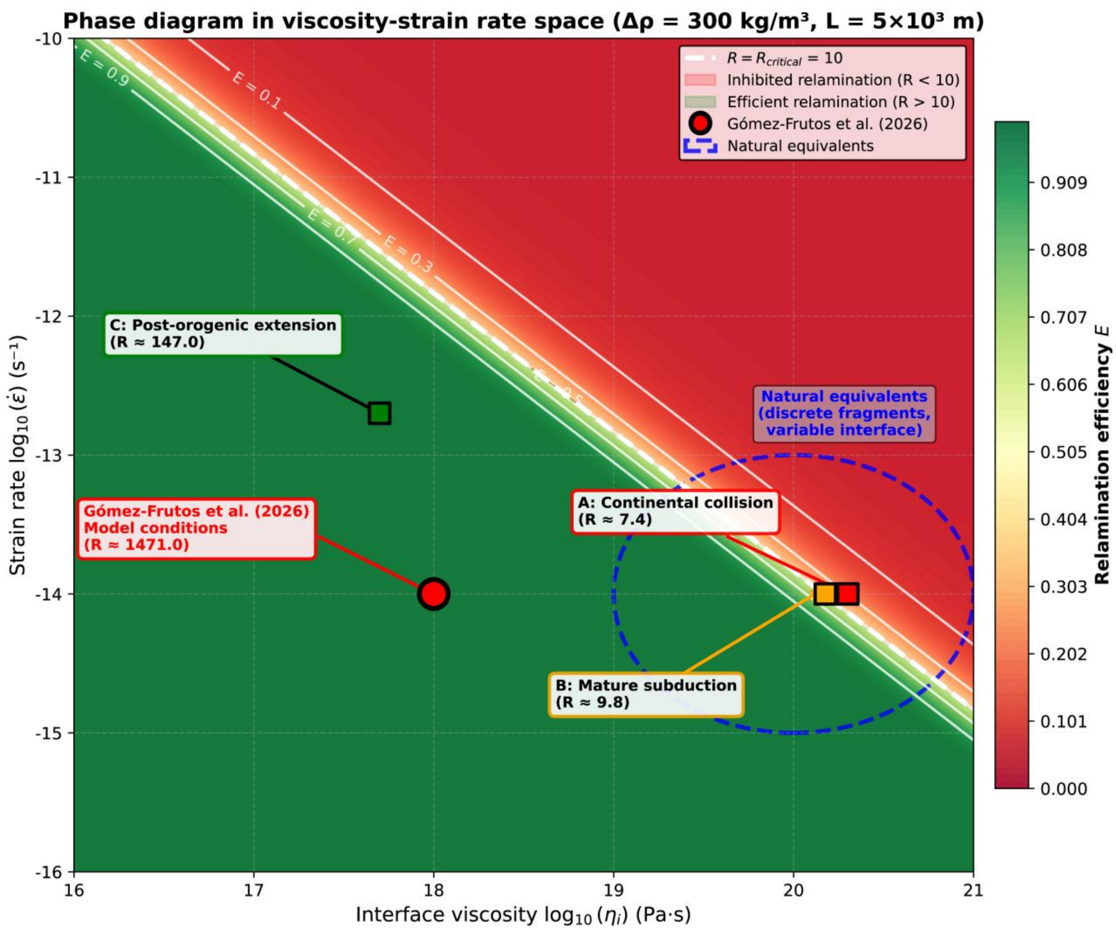

Figure 3

Figure 3. Phase diagram in interface viscosity–strain-rate space (model prediction). Contours show constant efficiency values (E = 0.1, 0.3, 0.5, 0.7, 0.9) for density

contrast $\Delta\rho$ = 300 kg m^{-3} and fragment size $L = 5 \times 10^3$ m. The white dashed line marks $R = R_{critical} = 10$. The colour gradient transitions from red (inhibited relamination, $R < R_{critical}$) through yellow (transition zone) to green (efficient relamination, $R > R_{critical}$). Natural scenarios (A–C): A (continental collision): interface viscosity $\eta_i \approx 2 \times 10^{20}$ Pa s, strain rate $\dot{\varepsilon} \approx 10^{-14}$ s^{-1}, $R \approx 7.4$ (inhibited regime). B (mature subduction): interface viscosity $\eta_i \approx 1.5 \times 10^{20}$ Pa s, strain rate $\dot{\varepsilon} \approx 10^{-14}$ s^{-1}, $R \approx 9.8$ (near-critical regime). C (post-orogenic extension): interface viscosity $\eta_i \approx 5 \times 10^{17}$ Pa s, strain rate $\dot{\varepsilon} \approx 2 \times 10^{-13}$ s^{-1}, $R \approx 147$ (efficient regime). Model comparison: the red circle marks the conditions inferred from the numerical models of Gómez-Frutos et al. (2026) (~1.5 GPa, 1200 °C, homogeneous-mixture assumption), which fall at $R \approx 1471$ (well within the efficient regime under their simplified boundary conditions). The blue dashed ellipse represents natural equivalents with discrete fragments and variable interface conditions, which may frequently fall below the critical threshold due to localized high-viscosity domains or low strain rates. The broad transition zone (yellow) indicates that relamination efficiency is not binary but spans a continuum, with natural systems frequently operating near the critical threshold where small parameter changes produce large efficiency variations.

Figure 3 presents a phase diagram showing the boundaries between efficient relamination ($R > R_{critical}$), transitional relamination ($R \approx R_{critical}$), and mechanically inhibited relamination ($R < R_{critical}$) in the η_i–$\dot{\varepsilon}$ parameter space. The diagram reveals that:

- high-viscosity, low-strain-rate regimes (upper left) fall predominantly in the inhibited zone;
- low-viscosity, high-strain-rate regimes (lower right) favor efficient relamination;
- a broad transition zone occupies the central parameter space, where small changes in local conditions can switch the system between regimes.

Natural scenarios mapped onto the diagram include:

- A (continental collision): $\eta_i \approx 2 \times 10^{20}$ Pa s, $\dot{\varepsilon} \approx 10^{-14}$ s^{-1}, $R \approx 7.4$ (inhibited regime);
- B (mature subduction): $\eta_i \approx 1.5 \times 10^{20}$ Pa s, $\dot{\varepsilon} \approx 10^{-14}$ s^{-1}, $R \approx 9.8$ (near-critical regime);
- C (post-orogenic extension): $\eta_i \approx 5 \times 10^{17}$ Pa s, $\dot{\varepsilon} \approx 2 \times 10^{-13}$ s^{-1}, $R \approx 147$ (efficient regime).

The model conditions inferred from Gómez-Frutos et al. (2026) (~1.5 GPa, 1200 °C, homogeneous-mixture assumption) fall at $R \approx 1471$, well within the efficient regime under their simplified boundary conditions. However, natural equivalents with discrete fragments and variable interface conditions may frequently fall below the critical threshold due to localized high-viscosity domains or low strain rates.

3.4 Conceptual model comparison

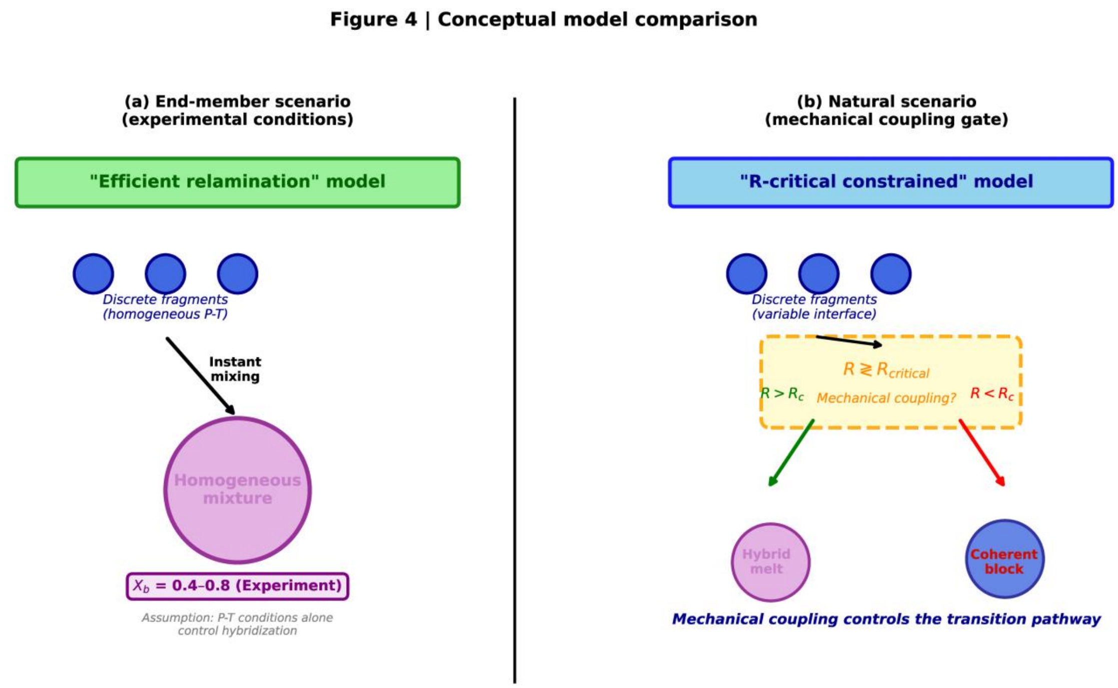

Figure 4

Figure 4. Conceptual model comparison. (a) Traditional "efficient relamination" model (left): discrete crustal fragments (blue circles) under homogeneous pressure–temperature conditions instantaneously mix into a homogeneous mixture (purple circle, X_b = 0.4–0.8) regardless of mechanical coupling strength. This end-member scenario corresponds to the experimental conditions of Gómez-Frutos et al. (2026) and assumes that pressure–temperature conditions alone control hybridization. (b) R-critical-constrained model (right): discrete crustal fragments (blue circles) with variable interface conditions encounter a mechanical coupling gate ($R \gtrless R_{critical}$) that controls the transition pathway. When $R > R_{critical}$ (green arrow), the interface yields and mechanical mixing produces hybrid melt (purple circle). When $R < R_{critical}$ (red arrow), the interface remains intact and fragments ascend as coherent blocks (blue circle) without significant hybridization. Mechanical coupling, not solely pressure–temperature, determines the geological outcome. This framework predicts that natural systems will exhibit a spectrum of mixing efficiencies depending on local mechanical conditions, rather than the binary efficient/inefficient dichotomy assumed in simplified models.

Figure 4 contrasts the traditional "efficient relamination" model with the R-critical-constrained model. The traditional model assumes that discrete crustal fragments under homogeneous P–T conditions instantaneously mix into a homogeneous mixture regardless of mechanical coupling strength. This end-member scenario corresponds to experimental conditions and assumes that P–T conditions alone control hybridization.

The R-critical-constrained model introduces a mechanical coupling gate ($R \gtrless R_{critical}$) that controls the transition pathway. When $R > R_{critical}$, the interface yields and mechanical mixing produces hybrid melt. When $R < R_{critical}$, the interface remains intact and fragments ascend as coherent blocks without significant mixing. Mechanical coupling, not solely P–T, determines the geological outcome. This framework predicts that natural systems will exhibit a spectrum of mixing efficiencies depending on local mechanical conditions, rather than the binary efficient/inefficient dichotomy assumed in simplified models.

3.5 Global relamination flux re-estimation

Figure 5 presents a Monte Carlo re-estimation (numerical simulation) of global relamination fluxes incorporating R-critical constraints. Hacker et al. (2011) estimated a continent-collision subduction rate of ~0.5 $km^3\ yr^{-1}$, of which the buoyant felsic fraction (~75 %) — approximately 0.35 $km^3\ yr^{-1}$ — could be relaminated to the base of the continental crust (their Fig. 9). This buoyant flux is unconstrained by mechanical coupling: it assumes that all buoyant fragments hybridize efficiently. Our Monte Carlo analysis (10,000 realizations with log-uniform parameter sampling across the natural ranges of Table 1) yields a mean efficiency of $E \approx 0.80$ (median ≈ 1.00), gating the effective continent-relamination flux to ~0.28 $km^3\ yr^{-1}$ (Fig. 5b).

Over 2.7 Ga of Earth history, the cumulative relaminated volume drops from ~$9.45 \times 10^8\ km^3$ (unconstrained buoyant flux) to ~$7.55 \times 10^8\ km^3$ (R-critical-constrained). This indicates that mechanical coupling constraints reduce the effective relamination flux by approximately 20 %, with implications for continental growth rates and geochemical budgets.

Variance decomposition (squared Spearman rank correlations, normalised; Sobol first-order indices as a robustness check) reveals:

- interface viscosity and strain rate contribute statistically equal, dominant shares of the variance in efficiency (~45 % each);
- fragment size contributes ~10 % of the variance;
- density contrast contributes <1 % of the variance.

This equality of the viscosity and strain-rate shares is not a numerical artifact but an exact symmetry of the formulation: both parameters enter the denominator of Eq. (1) multiplicatively and both are sampled log-uniformly over four decades. The sensitivity hierarchy therefore indicates that improving constraints on interface rheology *and* on the strain-rate field at depth are equally high priorities for future research.

4. Discussion

4.1 Model–observation convergence does not imply mechanistic uniqueness

We acknowledge that numerical models of relamination reproduce key natural observations, including post-collisional magmatic timing and geochemical signatures. However, model–observation convergence does not guarantee mechanistic uniqueness. Our R-critical analysis demonstrates that the same geochemical signatures could arise from alternative scenarios, such as:

1. inefficient, long-duration relamination below R-critical, where small but sustained hybrid contributions accumulate over geological time;
2. partial melting of detached lithospheric mantle with minimal crustal contribution, producing similar trace-element signatures through different pathways;
3. multi-stage processes involving initial delamination followed by limited relamination.

Without a quantitative discriminator like R-critical, the interpretation of post-collisional magmatism remains underdetermined. The R-critical framework provides exactly such a discriminator, enabling researchers to distinguish between mechanically efficient and inefficient regimes based on observable parameters.

4.2 The interface gap in integrated approaches

We identify a critical "interface gap" in integrated numerical–experimental approaches: numerical models output P–T–t trajectories and deformation geometries, while experiments require pre-homogenized mixtures as input. The physical process bridging these scales — mechanical mixing at the crust–mantle interface — is precisely what R-critical quantifies.

The experimental conditions of Gómez-Frutos et al. (2026) (1.5 GPa, 1200 °C, homogeneous mixtures) represent an end-member scenario where mechanical mixing is complete. Natural relamination, however, begins with discrete fragments. The R-critical framework defines the physical conditions under which these fragments can evolve toward the experimental end-member. This is not a criticism of experimental approaches, but rather a necessary scaling step to connect laboratory conditions to geological reality.

4.3 Global relamination flux reconsidered

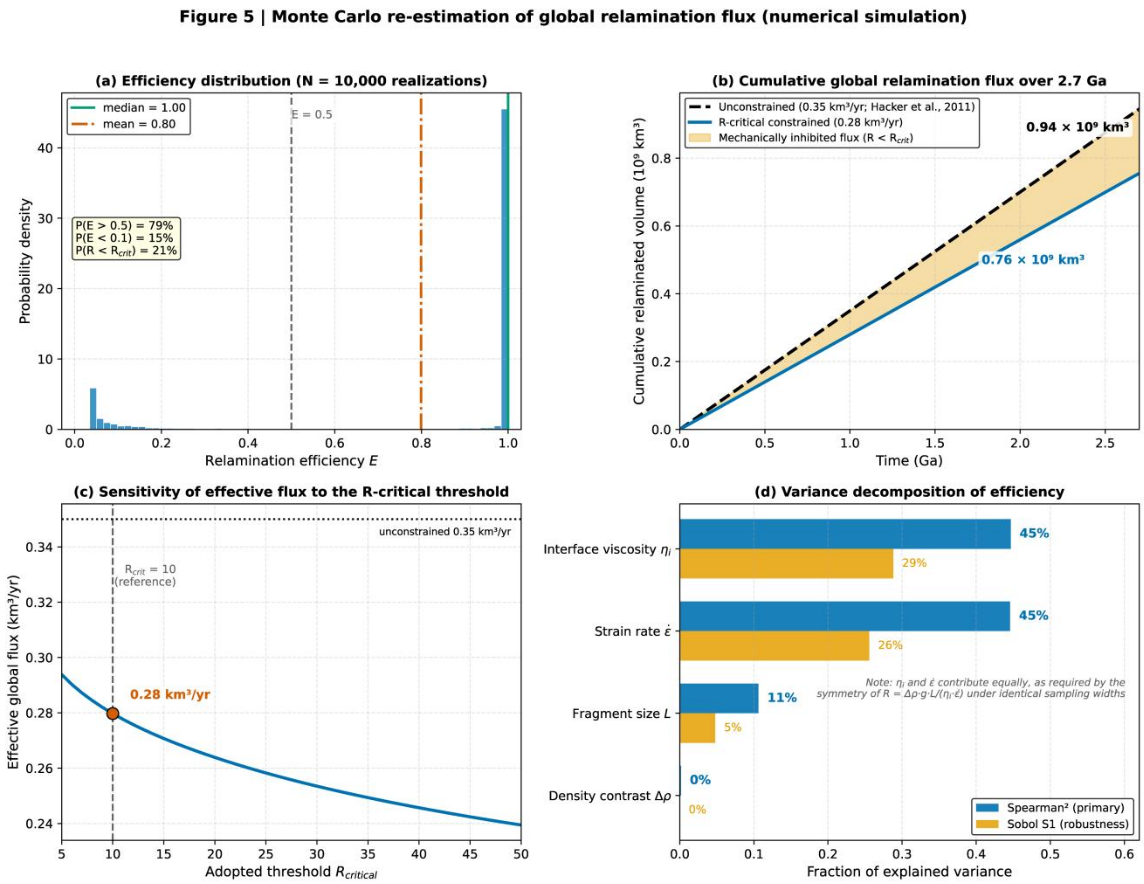

Figure 5

Figure 5. Monte Carlo re-estimation of the global relamination flux (numerical simulation). (a) Probability density distribution of the relamination efficiency E from 10,000 Monte Carlo realizations with log-uniform parameter sampling across the natural ranges (η_i = 10^{17}–10^{21} Pa s, $\dot{\varepsilon}$ = 10^{-16}–10^{-12} s^{-1}, L = 10^3–10^5 m, $\Delta\rho$ = 200–500 kg m^{-3}). The median efficiency is E ≈ 1.00 (mean E ≈ 0.80); 79 % of realizations yield E > 0.5, and 21 % fall below the critical threshold. The vertical dashed line marks E = 0.5 (transition midpoint). (b) Cumulative global relamination flux over 2.7 Ga. The unconstrained buoyant continent-relamination flux (0.35 km^3 yr^{-1}; Hacker et al., 2011, their Fig. 9) yields ~9.45 × 10^8 km^3 (black dashed line). The R-critical-constrained estimate (~0.28 km^3 yr^{-1}) yields ~7.55 × 10^8 km^3 (blue line). The shaded orange region represents the unrealized flux mechanically inhibited at $R < R_{critical}$. (c) Sensitivity of the effective global flux to the adopted $R_{critical}$ threshold. As $R_{critical}$ increases from 5 to 50, the effective flux decreases from ~0.29 to ~0.24 km^3 yr^{-1}; the conclusion of a mechanically gated flux is robust to a factor-of-five change in the threshold. The vertical dashed line marks our reference value $R_{critical}$ = 10. (d) Variance decomposition from the Monte Carlo sensitivity analysis (squared Spearman rank correlations, normalised; Sobol first-order indices shown as a robustness check). Interface viscosity (η_i) and strain rate ($\dot{\varepsilon}$) contribute

statistically equal shares (~45 % each), fragment size (L) ~10 %, and density contrast ($\Delta\rho$) <1 %, reflecting the exact symmetry of Eq. (1) under identical log-uniform sampling widths.

Hacker et al. (2011) estimated a continent-collision subduction rate of ~0.5 $km^3\ yr^{-1}$ and, after excluding the negatively buoyant mafic fraction, a potential continent-relamination flux of ~0.35 $km^3\ yr^{-1}$ (their Fig. 9). If R-critical constraints reduce the effective efficiency by approximately 20 % for natural parameter ranges (mean efficiency $E \approx 0.80$; Fig. 5a), the integrated contribution over 2.7 Ga drops from ~9.45×10^8 km^3 (unconstrained) to ~7.55×10^8 km^3 (R-critical-constrained). For context, Hacker et al. (2011) estimated that relamination across all four tectonic settings (sediment subduction, arc subduction, subduction erosion, and continent subduction) totals ~2.7–3.6 $km^3\ yr^{-1}$ — sufficient, in principle, to reprocess the entire continental crust (~6×10^9 km^3) within ~2.7 Ga; continent subduction is the smallest of the four contributors. This moderate reduction indicates that relamination remains a significant process, but its efficiency is mechanically gated rather than universally efficient. This has implications for:

- **continental growth rates:** if relamination contributes less than unconstrained estimates suggest, alternative mechanisms (arc magmatism, plume magmatism) may account for a larger proportion of crustal growth;
- **geochemical budgets:** the crustal recycling rate inferred from isotopic systems (e.g., Nd, Hf) may need recalibration where mechanical gating is strong;
- **thermal evolution:** reduced relamination fluxes imply less crustal material cycling through the mantle, affecting long-term thermal budgets.

4.4 Testable predictions

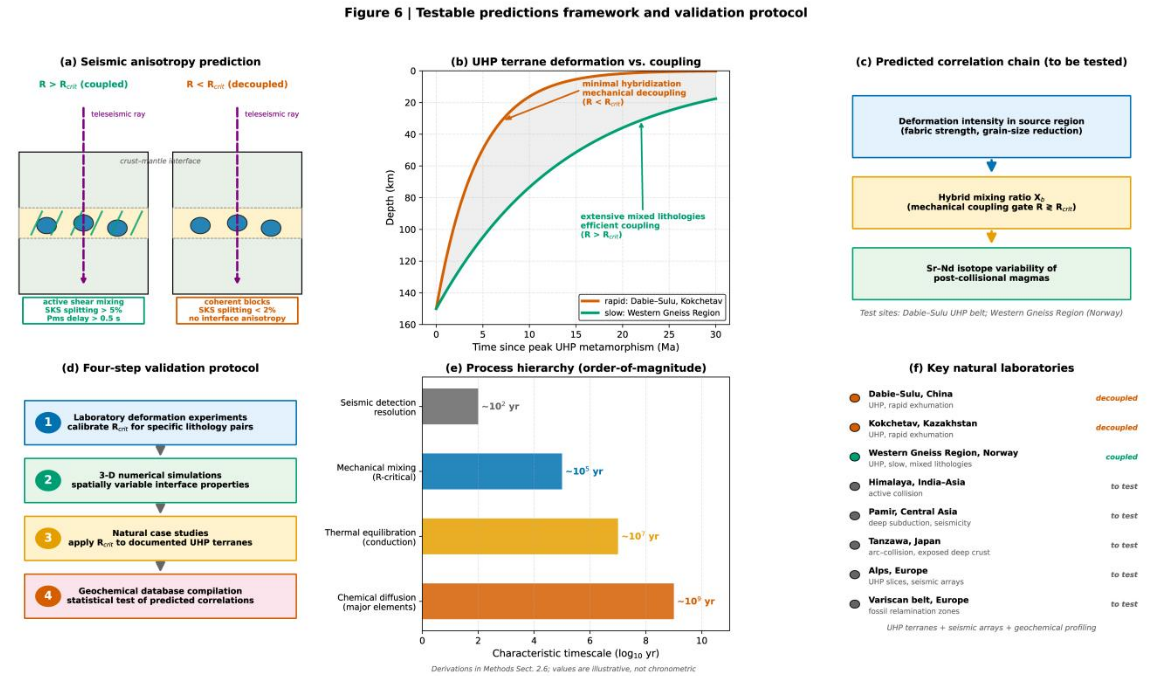

Figure 6

Figure 6. Testable predictions framework and validation protocol. (a) Seismic anisotropy prediction: regions with $R > R_{critical}$ (green) should exhibit active shear mixing with SKS splitting > 5 % and Pms delay > 0.5 s. Regions with $R < R_{critical}$ (red) should show coherent blocks with SKS splitting < 2 % and no anisotropy. Testable via seismic arrays at UHP terrane margins. (b) UHP terrane deformation: rapidly exhumed UHP terranes with minimal hybridization (e.g., Dabie–Sulu, Kokchetav) indicate mechanical decoupling ($R < R_{critical}$). Slowly exhumed terranes with extensive mixed lithologies (e.g., Western Gneiss Region, Norway) indicate efficient coupling ($R > R_{critical}$). (c) Post-collisional magma chemistry: predicted correlation chain (to be tested) — deformation intensity in the source region → hybrid mixing ratio (X_b) → Sr–Nd isotope variability. Test sites: Dabie–Sulu UHP belt, Western Gneiss Region (Norway). (d) Proposed four-step validation protocol: (1) laboratory deformation experiments to calibrate $R_{critical}$ for specific lithology pairs; (2) 3-D numerical simulations with spatially variable interface properties; (3) natural case studies applying $R_{critical}$ to well-documented UHP terranes; (4) geochemical database compilation and statistical testing of predicted correlations. (e) Process hierarchy: characteristic timescales (order-of-magnitude estimates based on standard physical parameters; see Sect. 2.6 for derivations). Mechanical mixing (R-critical): $\sim 10^5$ yr; thermal equilibration (conduction): $\sim 10^7$ yr; chemical diffusion (major elements): $\sim 10^9$ yr; seismic detection resolution: $\sim 10^2$ yr. (f) Key natural laboratories for testing the R-critical framework: Dabie–Sulu (China), Western Gneiss Region (Norway), Kokchetav (Kazakhstan), Himalaya (India–Asia), Pamir (Central Asia), Tanzawa (Japan), Alps (Europe), Variscan belt (Europe). These

localities provide the UHP terranes, seismic arrays, and geochemical profiling necessary for comprehensive validation.

The R-critical framework generates specific, testable predictions (Fig. 6):

1. **Seismic anisotropy:** regions where $R > R_{critical}$ should exhibit crust–mantle interface anisotropy consistent with active shear mixing (SKS splitting > 5 %, Pms delay > 0.5 s). Regions where $R < R_{critical}$ should show coherent, unmixed crustal blocks with weak or no anisotropy.
2. **UHP terrane deformation:** rapidly exhumed UHP terranes with minimal hybridization (e.g., Dabie–Sulu, Kokchetav) may indicate mechanical decoupling ($R < R_{critical}$), while slowly exhumed terranes with extensive mixed lithologies (e.g., Western Gneiss Region, Norway) may indicate efficient coupling ($R > R_{critical}$).
3. **Post-collisional magma chemistry:** magmas from relamination-dominated systems should show systematic correlations between mechanical coupling indicators (e.g., deformation intensity in source regions, quantified through fabric strength or grain-size reduction) and hybrid mixing ratios (X_b), as well as Sr–Nd isotope variability.
4. **Validation protocol:** we propose a four-step validation protocol: (i) laboratory deformation experiments to calibrate R-critical for specific lithology pairs; (ii) 3-D numerical simulations with spatially variable interface properties; (iii) natural case studies applying R-critical to well-documented UHP terranes; (iv) geochemical database compilation and statistical testing of predicted correlations.

4.5 Limitations and future directions

Our framework involves several simplifications that warrant acknowledgment:

1. **Dimensionality:** R-critical is a 1-D parameter that reduces complex 3-D thermomechanical processes to a single number. Like the Reynolds number or Rayleigh number, its value lies in providing a first-order screening tool, not in replacing 3-D modeling. Future work should explore tensorial extensions of R-critical for anisotropic viscosity fields.
2. **Constant parameters:** we treat $\Delta\rho$, η_i, and $\dot{\varepsilon}$ as constant for each scenario, whereas natural systems exhibit spatial and temporal variability. Time-dependent R-critical evolution during orogenic cycles remains an open question.
3. **Single R-critical value:** we adopt a reference $R_{critical}$ = 10.0 based on Vogt et al. (2013), but this value may vary with specific lithological compositions, P–T conditions, and melt fraction. Experimental calibration for specific crust–mantle lithology pairs is urgently needed. We note, however, that our central conclusion is robust to a factor-of-five change in the adopted threshold (Fig. 5c).

4. **No melt migration:** our model addresses mechanical mixing but does not explicitly treat melt segregation and migration after hybridization. Coupling R-critical with two-phase flow models (e.g., McKenzie, 1984) represents a natural extension.

5. Conclusions

We introduce the R-critical dimensionless parameter as a quantitative framework for evaluating mechanical coupling at the crust–mantle interface during continental relamination. Our analysis demonstrates that:

1. Relamination efficiency is fundamentally controlled by mechanical coupling, not solely by pressure–temperature conditions.
2. Efficient mechanical mixing is common but not universal: the median natural scenario is mechanically efficient, but a substantial minority (~21 %) of the sampled parameter space falls below the critical threshold for efficient hybridization.
3. The effective continent-relamination flux is mechanically gated to ~0.28 km^3 yr^{-1}, about 20 % below the unconstrained buoyant flux of ~0.35 km^3 yr^{-1} (Hacker et al., 2011, their Fig. 9), with implications for continental growth rates and geochemical budgets.
4. Interface viscosity and strain rate exert statistically equal, dominant control on efficiency — an exact symmetry of the formulation — so that rheological and tectonic constraints are of equal priority for future research.
5. The framework provides testable predictions for seismic, structural, and geochemical observations, and fills a theoretical gap between numerical model outputs and experimental petrology inputs, transforming the qualitative narrative of relamination into a parameterized, testable model.

This framework enables quantitative assessment of relamination's role in continental crust recycling and provides a foundation for future integrated geodynamic–petrological studies.

Code availability

All numerical simulation code, input parameters, and figure generation scripts used in this study (repository v2.0, including the Monte Carlo module `monte_carlo.py` and the scripts for Figs. 5 and 6) are available at GitHub (https://github.com/peter-clogite/R_Critical_Relamination) and archived at Zenodo under Concept DOI https://doi.org/10.5281/zenodo.20446103 (always resolves to the latest version). This preprint corresponds to Zenodo v2.0 (Version DOI: https://doi.org/10.5281/zenodo.21545544) under the MIT License. The repository includes a unit test suite (59 tests) verifying asymptotic behavior, monotonicity, regime classification, and seed-level reproducibility of all reported results, together with the complete mathematical derivation, the sensitivity analysis report, and the proposed validation protocol.

Data availability

No new observational or experimental data were generated in this study. The complete Monte Carlo output (10,000 realizations), the R-critical threshold sweep, and the variance decomposition are distributed with the code repository (`monte_carlo_realizations.csv`, `rcritical_sweep.csv`, `variance_decomposition.csv`, `monte_carlo_summary.json`; see Code availability). All parameter values are sourced from the published literature cited in the text.

Author contribution

SC: conceptualization, methodology, investigation, formal analysis, writing – original draft. XD: writing – review and editing. Both authors have read and approved the final manuscript.

Competing interests

The authors declare that they have no conflict of interest.

Acknowledgements

We thank colleagues at the Urumqi Natural Resources Survey and the Innovation Base of Metallogenic Prediction and Prospecting for constructive discussions. We acknowledge the use of Kimi (Moonshot AI; versions K2.6 and K3) for code implementation assistance and language polishing; all scientific hypotheses, theoretical framework development (including the R-critical concept, efficiency curves, and phase diagram design), data interpretation, and conclusions were independently developed by the authors. The authors take full responsibility for the scientific content.

This work was supported by the Regional Collaborative Innovation Special Project (Science and Technology Assistance Program for Xinjiang) and the Key Research and Development Program of Xinjiang Uygur Autonomous Region, under Grant Nos. 2026E02012 and 2024B03009, respectively. The funders had no role in study design, data collection and analysis, decision to publish, or manuscript preparation.

References

Christensen, N. I., and Mooney, W. D.: Seismic velocity structure and composition of the continental crust: A global view, J. Geophys. Res.-Sol. Ea., 100(B6), 9761–9788, https://doi.org/10.1029/95JB00259, 1995.

Gerya, T. V., Perchuk, L. L., Maresch, W. V., and Willner, A. P.: Inherent gravitational instability of hot continental crust: Implications for doming and diapirism in granulite facies terrains, in: Gneiss Domes in Orogeny, edited by: Whitney, D. L., Teyssier, C., and Siddoway, C. S., Geological Society of America Special Paper 380, 97–115, https://doi.org/10.1130/0-8137-2380-9.97, 2004.

Gómez-Frutos, D., Castro, A., Balázs, A., and Gerya, T. V.: Continental evolution influenced by relamination of deeply subducted continental crust, Nat. Geosci., 19, 589–595, https://doi.org/10.1038/s41561-026-01963-w, 2026.

Hacker, B. R., Kelemen, P. B., and Behn, M. D.: Differentiation of the continental crust by relamination, Earth Planet. Sc. Lett., 307(3–4), 501–516, https://doi.org/10.1016/j.epsl.2011.05.024, 2011.

Hirth, G., and Kohlstedt, D. L.: Rheology of the upper mantle and the mantle wedge: A view from the experimentalists, in: Inside the Subduction Factory, edited by: Eiler, J., Geophys. Monogr. Ser., 138, AGU, Washington, DC, 83–105, https://doi.org/10.1029/138GM06, 2003.

Kelemen, P. B., and Behn, M. D.: Formation of lower continental crust by relamination of buoyant arc lavas and plutons, Nat. Geosci., 9, 197–205, https://doi.org/10.1038/ngeo2662, 2016.

Kreemer, C., Blewitt, G., and Klein, E. C.: A geodetic plate motion and Global Strain Rate Model, Geochem. Geophy. Geosy., 15(10), 3849–3889, https://doi.org/10.1002/2014GC005407, 2014.

McKenzie, D.: The generation and compaction of partially molten rock, J. Petrol., 25(3), 713–765, https://doi.org/10.1093/petrology/25.3.713, 1984.

Vogt, K., Castro, A., and Gerya, T.: Numerical modeling of geochemical variations caused by crustal relamination, Geochem. Geophy. Geosy., 14(2), 470–487, https://doi.org/10.1002/ggge.20072, 2013.

Zhang, Y.: Diffusion in minerals and melts: theoretical background, Rev. Mineral. Geochem., 72, 5–59, https://doi.org/10.2138/rmg.2010.72.2, 2010.